JCEC
THE JOURNAL OF ENGINEERING AND EXACT SCIENCES

OPEN ACCESS

The Journal of Engineering and Exact Sciences – jCEC, Vol. 08 N. 05 (2022)
journal homepage: https://periodicos.ufv.br/jcec
eISSN: 2527-1075
ISSN: 2446-9416

Thermal and Fluid Flow Performance Analysis of Tubular Microchannel Heat Sinks with Inward Protrusions and Nanofluids

Análise de desempenho de fluxo térmico e de fluido de dissipadores de calor tubulares de microcanais com saliências internas e nanofluidos

Article Info:
Article history: Received 2022-01-04 / Accepted 2022-03-20 / Available online 2022-04-22
doi: 10.18540/jcecvl8iss5pp14233-01e

Ibrahim Ademola Fetuga
ORCID: https://orcid.org/0000-0002-1943-4234
University of Lagos, Nigeria
E-mail: fetugaebraheem@gmail.com
Olabode Thomas Olakoyejo
ORCID: https://orcid.org/0000-0001-9942-1339
University of Lagos, Nigeria
E-mail: oolakoyejo@unilag.edu.ng
Antônio Marcos de Oliveira Siqueira
ORCID: https://orcid.org/0000-0001-9334-0394
Federal University of Viçosa, Brazil
E-mail: antonio.siqueira@ufv.br
Joshua Kolawole Gbegudu
ORCID: https://orcid.org/0000-0003-2417-2520
University of Lagos, Nigeria
E-mail: jk.gbegudu@gmail.com
Ebenezer Aderibigbe Adeyemi
ORCID: https://orcid.org/0000-0001-5487-1248
University of Lagos, Nigeria
E-mail: ebenezer.adeyemiiii@gmail.com

Resumo

Neste trabalho, a aplicação de saliências e nanofluidos para melhorar o desempenho do dissipador de calor tubular-microcanal (MCHS) é proposta e investigada computacionalmente. As equações tridimensionais de Navier-Stokes e de energia foram resolvidas numericamente usando o método de volumes finitos incorporado ao pacote de software ANSYS (Fluent). Foram investigados os efeitos de diferentes tipos de nanofluido (Al_2O_3, CuO, ZnO em água pura), a fração volumétrica das nanopartículas (0% a 4%) e a altura da saliência (2 μm-6 μm) em dissipadores de calor de microcanais sob a condição de estado estacionário e números de Reynold (400-2 000) com fluxo de calor constante de 9×10^6 W/m^2. Foi revelado que o desempenho térmico melhorou à medida que a altura da saliência aumentou. Em *Re* = 2 000, para Al_2O_3 nanofluido (NAN) com uma fração de volume (Ø) de 4% e uma altura de protrusão (H) de 2 μm a 6 μm produziu um valor de desempenho térmico de 1,59, 1,68, 1,77, 1,86, e 1,96 vezes a do MCHS sem a saliência, respectivamente. Além disso, em uma fração de volume de 4%, altura de protrusão de 6 μm e número de Reynolds de 800, os nanofluidos Al_2O_3, CuO e ZnO produziram um valor de desempenho térmico de 1,79, 1,08 e 1,07 vezes o da água pura, respectivamente. Além disso, em um número de Reynolds de 400 e uma fração de volume de 4%, o nanofluido Al_2O_3-água reduziu a temperatura máxima da parede MCHS em 4%, enquanto os nanofluidos CuO e ZnO diminuíram a temperatura máxima da parede MCHS em 0,5%. e 0,48% em relação à água pura, respectivamente. No entanto, para todos os casos de fração volumétrica (1% a 4%), houve uma tendência de aumento no valor do desempenho térmico para a

faixa de números de Reynolds de 400≤*Re*≤800, e diminuição com a faixa de números de Reynolds de 800≤ *Re*≤2 000.
Palavras-chave: Simulação. Saliência. Nanofluidos. Dissipador de calor microcanal. Performance térmica.

Abstract
In this work, the application of protrusions and nanofluids to improve the performance of tubular-microchannel heat sink (MCHS) is proposed and investigated computationally. The three-dimensional Navier-Stokes and energy equations were solved numerically using the finite volume method incorporated into the ANSYS (Fluent) software package. The effects of different types of nanofluid (Al_2O_3, CuO, ZnO in pure water), the volume fraction of the nanoparticles (0% to 4%) and height of the protrusion ($2\ \mu m - 6\ \mu m$) on microchannel heat sinks were investigated under the steady-state condition and Reynold numbers ($400 - 2\,000$) with constant heat flux of $9 \times 10^6\ W/m^2$. It was revealed that thermal performance improved as protrusion height increased. At $Re = 2\,000$, for Al_2O_3 nanofluid (NAN) with a volume fraction ($\emptyset$) of 4% and a protrusion height (H) of 2 µm to 6 µm yielded a thermal performance value of 1.59, 1.68, 1.77, 1.86, and 1.96 times that of MCHS without the protrusion, respectively. In addition, at a volume fraction of 4%, protrusion height of 6 µm and Reynolds number of 800, the Al_2O_3, CuO and ZnO nanofluids yielded a thermal performance value of 1.79, 1.08, and 1.07 times that of pure water, respectively. Furthermore, at a Reynolds number of 400 and a volume fraction of 4%, the Al_2O_3–water nanofluid reduced the maximum temperature of the MCHS wall by 4%, whereas CuO- and ZnO-nanofluids decreased the MCHS wall maximum temperature by 0.5% and 0.48% when compared to pure water, respectively. However, for all the cases of volume fraction (1% to 4%), there was an increase trend in the value of thermal performance for the Reynolds number range of $400 \leq Re \leq 800$, and decrease with the Reynolds number range of $800 \leq Re \leq 2\,000$.
Keywords: Simulation. Protrusion. Nanofluids. Microchannel Heat Sink. Thermal Performance.

1. Introduction

Cooling technology is needed to dissipate the heat generated by electronics such as computers, to maintain and keep them within an acceptable operating condition (temperature). This is necessary to avoid overheating, which could subject the components of the system to malfunction or even unexpected failure if not properly taken care of. Adequate cooling is therefore required in the design of the electronics or other heat-generating devices to effectively achieve the overall excellent performance of these systems (Cong, Ozaki, Machado, & Das, 2018). The use of heat sinks to cool heat-generating devices is not new; it has been in existence over the decades. They are generally known to have a high heat transfer coefficient, and are smaller in size and volume with little space required for coolant. Heat sinks, when coupled with nanofluids, generate a hydrodynamic flow in a particular pattern that reduces the temperature rise in devices that generate the heat (Pordanjani et al., 2021; Yan, Aghakhani, & Karimipour, 2020). Microchannel heat sinks (MCHS) mostly have a large array of microchannels with a size/dimension between 10 μm and 1000 μm where coolant such as smart fluid or nanofluid (NAN) is compelled to flow through to minimize the heat generated on the surface of the hot source.

Over the years, extensive studies have been proposed and performed by researchers on heat sinks. (Heris, Etemad, & Esfahany, 2006) examined the impacts of CuO and Al_2O_3 NANs flowing through an annular tube subjected to a constant wall temperature. They discovered that increasing the volume percentage of the nanoparticle improved the heat transfer coefficient. (Marques & Kelly, 2004) studied the pressure drop and thermal performance of a pin-finned MCHS. They indicated that high thermal performance is achieved in the pin-finned type rather than the parallel plate type and further proposed a predictive model for the cooling performance of the pin-finned type. (Wang,

Houshmand, Elcock, & Peles, 2013) experimented on a MCHS with an array of pin fins of different cross-sections under high Reynolds numbers. They concluded that a triangular cross-section pin-fin provides higher thermal performance. (Gong, Lu, Li, & Xu, 2016) examined the thermal characteristics of a dimpled MCHS. They reported that the Nusselt number increased by 15% in the dimpled MCHS as compared to the plain channel. (Ahmed, Shuaib, Yusoff, & Al-Falahi, 2011) performed a numerical simulation on thermal characteristics in a wavy MCHS using Cu/H_2O NAN under a laminar flow conditions and constant temperature at different nanoparticle concentrations. They indicated that both the heat transfer coefficient and pressure drop increase as the volume fraction of the nanoparticles increases. (Uday Kumar et al., 2021) studied the cooling performance of graphene/water NAN in a MCHS made of silicon. They reported that an increase in both volume fraction and flow velocity improved the cooling efficiency of the MCHS. (Munimathan et al., 2021) performed experiments on the thermal characteristics of Al_2O_3/H_2O NAN flowing through a MCHS. They revealed that at a volume fraction of 0.25%, about 32.5% increase in thermal resistance was achieved in contrast to deionized water. (Khetib, Abo-Dief, Alanazi, Cheraghian, et al., 2021) employed CAMSOL software to examine the heat transfer characteristics of Al_2O_3/H_2O nanofluid in a corrugated MCHS. From their results, it was found that at a 0.0437% nanoparticle concentration and a Reynolds number of 807.87, a best performance of MCHS was achieved. (Ali, Angelino, & Rona, 2021) numerically analyzed the hydrothermal performance of various arrangements of the fins in the MCHS operating with Al_2O_3/H_2O NAN. They reported that the best performance was obtained in a zig-zag fin as compared to other fin configurations. (Mohamad Hafzan Mohamad Jowsey, Natrah Kamaruzaman, & Mohsin Mohd Sies, 2021) numerically examined the hydrothermal profile of Al_2O_3/H_2O NAN in a MCHS consisting of multiple layers. They concluded that Al_2O_3/H_2O nanofluid had a better heat transfer rate than that of pure water, but its higher pressure drop still remained a setback. (Adham & Mohammed, 2021) numerically assessed the flow and thermal behavior of Al_2O_3/NH_3 and Al_2O_3/H_2O based nanofluids in a rectangular MCHS. The findings from their results revealed that Al_2O_3/NH_3 nanofluid provides a best performance than both Al_2O_3/H_2O and pure water. Raghuveer and Harish (Rhaghuveer & Harish, 2021) analyzed the impacts of various nanofluids on rectangular MCHS. They suggested that TiO_2 NAN yielded a highest heat transfer coefficient, followed by CuO, Al_2O_3, Fe_3O_4, and pure water, respectively. (Khetib, Abo-Dief, Alanazi, Sajadi, et al., 2021) adopted a CFD approach to examine the cooling performance of a wavy MCHS with a Al_2O_3 and CuO NANs. They indicated that high thermal resistance was obtained in Al_2O_3 NAN compared to CuO NAN.

From the previous studies, it can be deduced that tubular MCHS with protrusion is rarely investigated. Therefore, this research aims to numerically assess the influence of various heights of protrusion, nanofluid types, and nanoparticle concentrations on the thermal performance of the tubular MCHS subjected to constant wall heat flux at Reynolds number ranging from 400 to 2000.

2. Methodology

2.1 Geometry Description

The geometry was modeled in ANSYS Design Modeler with Fig. 1(a)-(d) illustrating the various views of geometry configuration used in this study. The nanofluid flowing through the three-dimensional tubular MCHS of finite length L with an external and internal diameter of D_1 and D_2 respectively, was considered. The MCHS is incorporated with a circular array of rectangular cross-section protrusions projected towards the center of the MCHS. Also, the array of protrusions (10 sets) extended laterally to the other end of the heat sink. The protrusion has a length (L_p), width (W_p) and a height (h_p) while the angle and the spacing between the center of each protrusion are θ and W_s, respectively. The wall of the MCHS was subjected to constant heat flux (q''_w). The parameters used for the geometry are shown in Table 1.

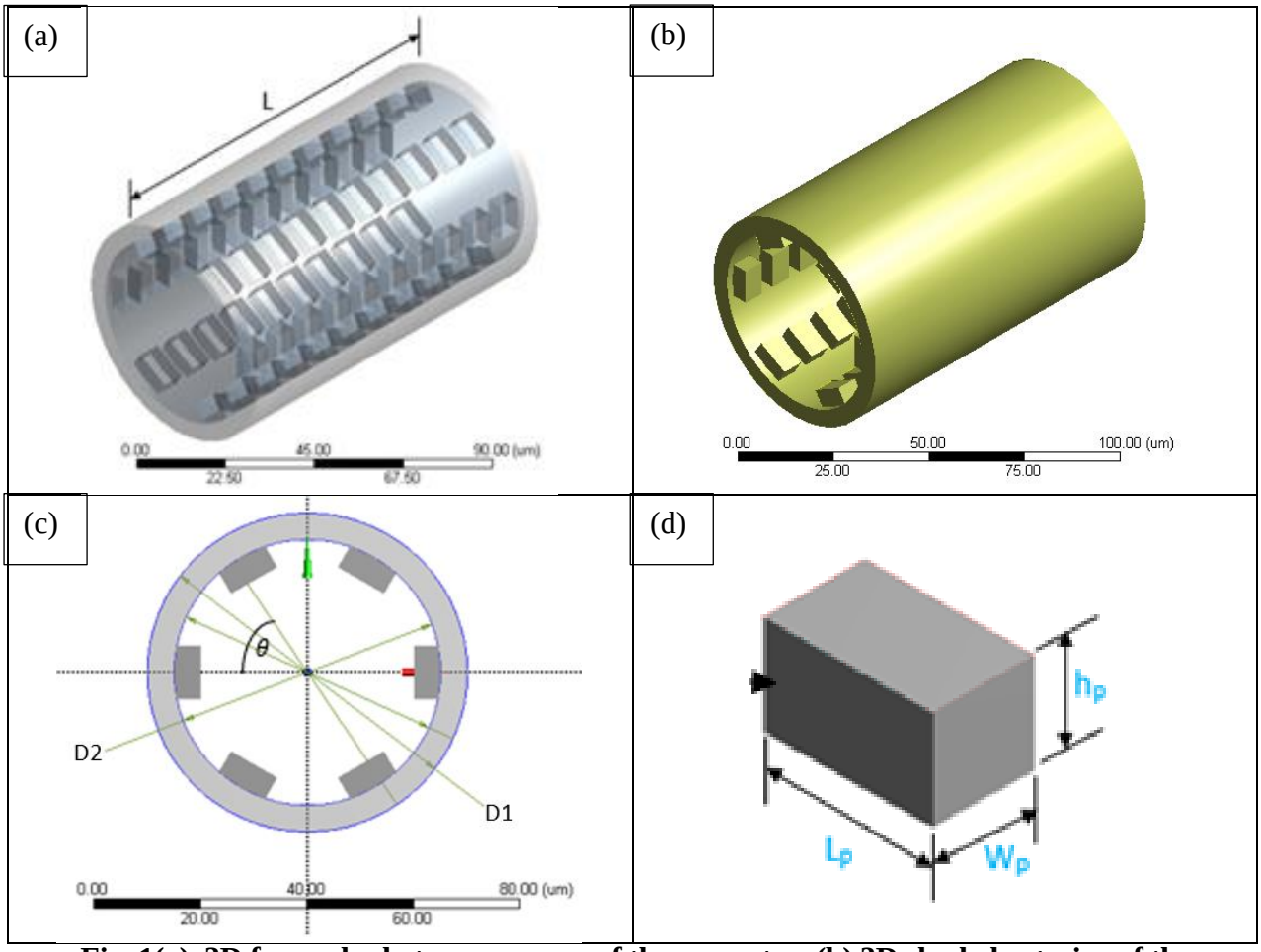

Fig. 1(a). 3D frozen body transparency of the geometry, (b) 3D shaded exterior of the schematic diagram, (c) End-view of the schematic diagram, (d) Zoom-out view of the protrusion

Table 1- Parameters of the geometry

Parameters	Dimension
$\mathbf{L}$	100 µm
$\mathbf{D_1}$	60 µm
$\mathbf{D_2}$	50 µm
$\boldsymbol{\theta}$	60^o
$\mathbf{L_p}$	10 µm
$\mathbf{W_p}$	6 µm
$\mathbf{h_p}$	2, 3, 4, 5 and 6 µm
$\mathbf{W_s}$	10 µm
$\mathbf{q''_w}$	9×10^6 W/m^2

2.2 Grid Generation

To obtain an accurate and concise numerical solution for this study within an optimized computational cost and resources. As shown in Fig. 2(a)-(b), a numerical discretization was conducted. The grids were generated using the ANSYS Meshing Tool and the unstructured patch conforming tetrahedron method was applied to the whole geometry. A refined mesh of an element

size of 0.0013 mm was applied to the MCHS while the protrusions were meshed to an element size of 0.0007 mm.

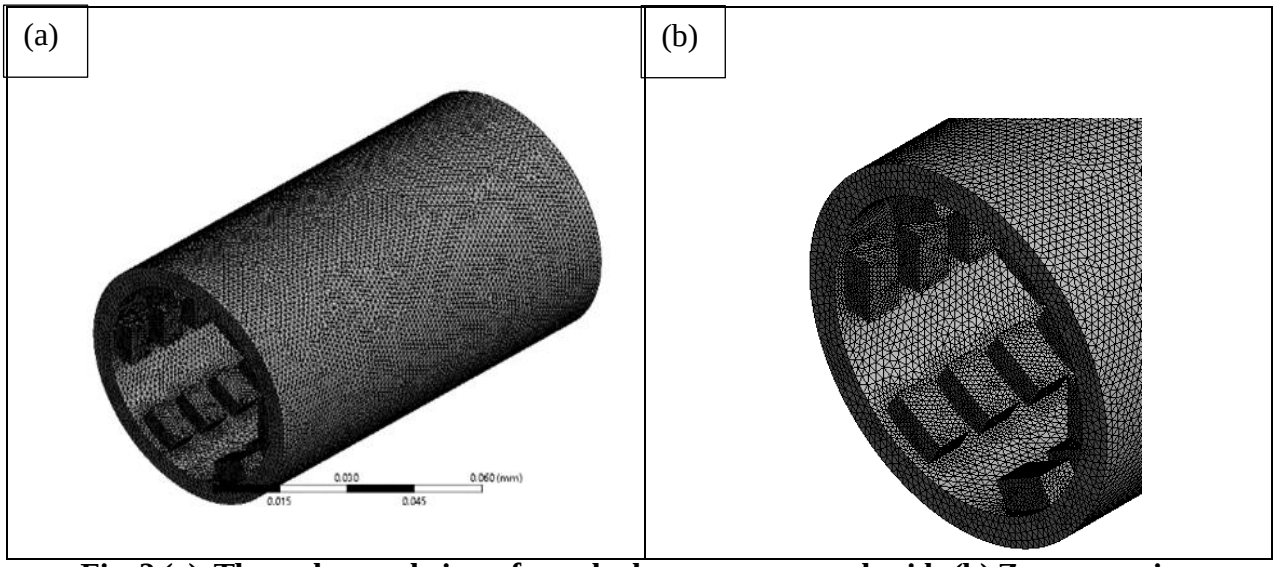

Fig. 2 (a). The orthogonal view of tetrahedron unstructured grids (b) Zoom-out view

2.3 Problem Formulation

This subsection discusses the governing equations, assumptions, and boundary conditions (see Table 3) used for this study. The 3D Navier-Stokes and energy equations with NAN properties were used to solve the problem. The governing equations were further simplified under the assumptions [17] listed below;

1. Steady, laminar, single phase, 3D incompressible NAN flow and heat transfer
2. The thermo-physical properties of the fluid and solid are constant.
3. Viscous dissipation is neglected.
4. Thermal radiation, natural convection, and magnetic force are ignored.

The governing equations can be expressed as follows;

Continuity equation

$$\nabla.\vec{u} = 0 \tag{1}$$

Momentum equation

$$\rho_{NF}(\vec{u}.\nabla)\vec{u} = -\nabla \mathrm{P} + \mu_{NF}\nabla^2\vec{u} \tag{2}$$

Energy equation

$$\rho_{NF}C_{p_{NF}}(\vec{u}.\nabla \mathrm{T}) = k_{NF}\nabla^2. \tag{3}$$

Nanofluid thermo-physical properties

A varied volume fraction $(1\% - 4\%)$ of Al_2O_3, CuO, ZnO NANs were used for this study. The effective thermo-physical properties (see Table 2) of the nanofluids are expressed below:

Density correlation (Manca, Nardini, Ricci, & Tamburrino, 2012)

$$\rho_{NAN=}(1-\phi)\rho_F + \phi\rho_{NP} \tag{4}$$

Specific heat correlation [18]

$$\rho_{NAN}C_{p_{NAN}} = (1-\phi)C_{p_F} + \phi C_{p_{NP}} \tag{5}$$

Dynamic viscosity (Masoumi, Sohrabi, & Behzadmehr, 2009)

$$\mu_{NAN} = \mu_F + \frac{\rho_{NP}V_B d_{NP}^2}{72C\delta} \tag{6}$$

Where δ represents boundary layer thickness and V_B is Brownian velocity, both could be defined below as:

$$V_B = \frac{1}{d_{NP}}\sqrt{\frac{18K_BT}{\pi\rho_{NP}d_{NP}}}, \qquad \delta = \sqrt[3]{\frac{\pi}{6\phi}}d_{NP} \tag{7}$$

Where K_B and d_{NP} represent Boltzmann constant and NP diameter

$$C = {\mu_F}^{-1}[(y_1 d_{NP} + y_2)\phi + (y_3 d_{NP} + y_4)] \tag{8}$$

Where the mean diameter of nanoparticles and is expressed in nanometer.

$$\begin{aligned} y_1 &= -0.0000011, \qquad y_2 = -0.0000028, \\ y_3 &= 0.00000009, \qquad y_4 = -0.00000039. \end{aligned} \tag{9}$$

Thermal conductivity (Chon, Kihm, Lee, & Choi, 2005)

To estimate the effective thermal conductivity of the NAN in Eq. (10), Brownian motion and mean-diameter of the nanoparticles is used;

$$k_{NAN} = k_F\left[164\emptyset^{0.746}\left(\frac{d_F}{d_{NP}}\right)^{0.369}\left(\frac{k_P}{k_F}\right)^{0.746}(Pr_{NAN})^{0.9955}(Re_{NAN})^{1.2321}\right] \tag{10}$$

Where Pr_{nf}, Re_{nf} and K_B are defined as:

$$Pr_{NAN} = \frac{\mu_{NAN}}{\rho_{NAN}\alpha_{NAN}}, \quad Re_{NAN} = \frac{\rho_{NAN}\,k_BT}{3\pi\mu_{NAN}^2 l_{MF}}, \quad K_B = 1.3807e^{-23} \tag{11}$$

Where l_{MF} represents mean-free path of the base fluid

Table 2- Thermo-physical properties for base fluid (water) and nanoparticles (NPs) at T=300K

Parameter	$\rho(kgm^{-3})$	$C_p(Jkg^{-1}K^{-1})$	$k(Wm^{-1}K^{-1})$	$\mu(Pa.s)$
Pure water	998.2	4 182	0.6	0.001003
Al_2O_3	3 970	765.0	40	-
ZnO	5 600	4 95.2	1.3	-
CuO	6 500	535.6	20	-

Table 3- Boundary Conditions

Boundary	Location	Condition
Hydrodynamics	Fluid/solid interface	$u = v = w = 0$
	Inlet: $z = 0, r = 0$	$u = v = 0$
		$U = U_{max}(1 - \frac{x^2 + z^2}{r^2})$
		$\frac{\partial u}{\partial r} = \frac{\partial v}{\partial r} = \frac{\partial w}{\partial r} = 0$
	Heat sink wall: $r = R_i(z)$	(No-slip condition) $u = v = w = 0$
	Outlet: $z = L$	$P_f = 0$
Thermal	Fluid/solid interface	$-k_s\left(\frac{\partial T_s}{\partial n}\right) = -k_f\left(\frac{\partial T_s}{\partial n}\right)$
	Inlet: $z = 0, r = 0$	$T_f = 300K, \frac{\partial T}{\partial r} = 0$
	Heat sink wall: $r = R_1$	$q_w = 9 \times 10^6 W/m^2$

Thus, Reynolds number [21]

$$Re = \frac{\rho_{NAN} U D_H}{\mu_{NAN}} \quad (12)$$

where U and D_H are inlet velocity and hydraulic diameter of the MCHS respectively

Nusselt number [21] is defined as

$$Nu = \frac{hD_H}{k_{NAN}} \tag{13}$$

Where h indicates heat transfer coefficient, k_{NF} represents effective thermal conductivity of nanofluid

Fanning friction factor (Aurangzeb et al., 2022) is expressed as;

$$f = \frac{\left(\frac{\Delta P}{L}\right)D_H}{2\rho_{NAN}} \tag{14}$$

Where $L\ and\ \Delta P$ is the length and pressure drop across the microchannel respectively.

Thermal performance (Chaurasia & Sarviya, 2021) is expressed as follow;

$$TP = \left[\left(\frac{Nu}{Nu_R}\right)\left(\frac{f}{f_R}\right)^{-\frac{1}{3}}\right] \tag{15}$$

Here, Nu_R and f_R indicate reference for Nusselt number (Nu) and Fanning friction (f) factor obtained from the case of MCHS without protrusions.

3. Numerical Procedures

ANSYS (Fluent) software package was used to solve the continuity, Navier-Stokes equation, and energy (1) to (3) while taking into consideration the boundary conditions and assumptions for the sake of simplicity. Under the steady-state condition, at a temperature of $300K$, a NAN flow through the inlet of the MCHS with fully developed velocity, and the outer wall of the MCHS was subjected to a constant heat flux of $9 \times 10^9\ \mathrm{W/m^2}$. For pressure-velocity coupling, the SIMPLEC algorithm was used, a Gauss cell-based scheme was used for the discretization scheme, the standard was set for pressure, a second-order upwind scheme was used to solve both momentum and energy equations, under-relaxation factors were set as default values, and all equations were set as convergence criteria of 1×10^{-7}.

4. Results and Discussion

4.1 Grid Independence Test

To effectively maximize the computation resources, a reasonable grid is determined by conducting a grid independence test on six grids of different elements and nodes. As shown in Table IV, the Nusselt number of Al_2O_3 NAN with a $\emptyset$ of 4% and $25\ nm$ nanoparticle size for Re of 400 was compared for different grids, it was revealed that by further increasing the grid size beyond **Mesh 4**, there was no significant change in Nu, even when the numerical values were rounded up to 8 decimal places. Therefore, **Mesh 4** was chosen for this computational study.

Table 4- Grid independence analysis
Nusselt number for Al_2O_3 at $d_{np} = 25$ nm, h = 6 µm and $Re = 400$

Mesh	Elements	Nodes	$\phi = 0\%$	$\phi = 1\%$	$\phi = 2\%$	$\phi = 3\%$	$\phi = 4\%$
Mesh 6	1904980	327051	28.94748194	34.55214921	40.10417281	45.81986499	51.64009321
Mesh 5	1618847	279244	28.94748190	34.55214527	40.10417266	45.81986408	51.64008111
Mesh 4	1275688	221773	28.94748172	34.55214491	40.10417264	45.81986491	51.64008417
Mesh 3	209274	216776	27.53972952	32.40263722	38.15220092	43.20937384	49.83541121
Mesh 2	182976	207219	25.22810283	30.44600202	35.17291109	40.74092364	46.43649001
Mesh 1	159614	145935	22.50283228	30.00720991	34.00347388	39.09293861	44.96859392

4.2 Validation of Model

The model is validated by comparing the simulated results of Al_2O_3/water NAN at a volume fraction of 4% flowing through a MCHS without protrusions with the numerical results of Maiga et al.(El Bécaye Maïga, Palm, Nguyen, Roy, & Galanis, 2005). As shown in Table V. A good agreement is observed in our simulated results with a minimum deviation of 0.5% and a maximum deviation of 7.6% from the numerical results of Maiga et al. [23]. This provides confidence in the accuracy of our proposed model.

Maiga et al. [23] correlation for NAN;

$$Nu = 0.085Re^{0.71}Pr^{0.35} \quad (16)$$

Table 5- Validation of the model
Nusselt number for Al_2O_3 at $d_p = 25\ nm$, $\phi = 4\%$ for a MCHS without protrusions

	Nu		
Re	**Maiga et al. (2006)**	**Present**	**Difference (%)**
400	18.37883003	19.44620725	5.80764513
800	30.06416582	32.37386160	7.682554015
1200	40.09349835	41.34826154	3.129592705
1600	49.17908623	49.43027670	0.510766849
2000	57.62176599	56.21856873	2.43518 613

4.3 Influence of Nanofluids Type

The impact of NANs on the wall temperature (T_w), Nusselt number (Nu), and the skin friction coefficient (f) at a volume fraction ($\emptyset$) of 4% and a nanoparticle size (d_{np}) of 25 nm on 6 μm protrusion height of tubular MCHS is illustrated in Figs. 3, 4, 5, and 6 respectively. Fig. 3 presents the distribution of T_w for varied Re and nanofluid types. For all cases of NAN, the T_w drops as the Re increases. Al_2O_3–water NAN gives the lowest T_w, followed by CuO NAN, whereas ZnO-water NAN exhibits the highest T_w. This is simply attributed to the effective thermal conductivity and viscosity properties. Quantitatively, at $Re = 400$, ϕ =4% and $d_{np} = 25\ nm$, using pure-water as a reference, the maximum temperature of the surrounding wall of MCHS using Al_2O_3-water NAN decreased by 4% while CuO and ZnO NAN decreased by 0.5% and 0.48%, respectively. Fig. 4 reveals the comparison of the Nu with the Re number for various NANs. It has been demonstrated that the Nu in nanofluids is higher than that of pure water, and this fact implies that heat transfer is enhanced in pure water by the addition of nanofluid. Furthermore, Nu increases with Re, where the

maximum value of Nu is obtained in Al_2O_3 NAN, followed by CuO, ZnO NAN, and pure water. The reason for this is that among the NANs, Al_2O_3 NAN tends to have the highest average velocity as a result of its low density, especially by forced convection. At $Re = 2\,000$, the heat transfer rate is enhanced by 40% in Al_2O_3 NAN, 8.7% in CuO NAN and 9% in ZnO NAN. The skin friction coefficient (f) decreases as the Re rises for all cases of NANs (see Fig. 5). Furthermore, it is evident that no significant change in the value of f is observed when compared to the base fluid (pure water) for all the NANs. This implies that adding the nanoparticles to the pure water (base fluid) does not enhance the skin friction factor. Fig. 6 reveals that thermal performance (TP) increases linearly with Re for both CuO and ZnO NAN, whilst different behavior is depicted in Al_2O_3 NAN. However, the thermal performance of the MCHS with Al_2O_3 NAN increases with Reynolds number at $400 \leq Re \leq 800$ (due to the dominating effect of heat transfer rate) and further decreases with Re at $800 \leq Re \leq 2\,000$ (as a result of the dominating effect of friction factor). The highest value of the TP of about 1.79 times that of pure water is obtained in Al_2O_3 NAN at $Re = 800$. Meanwhile, the difference in the values of TP for both CuO and ZnO for all ranges of Re can be neglected.

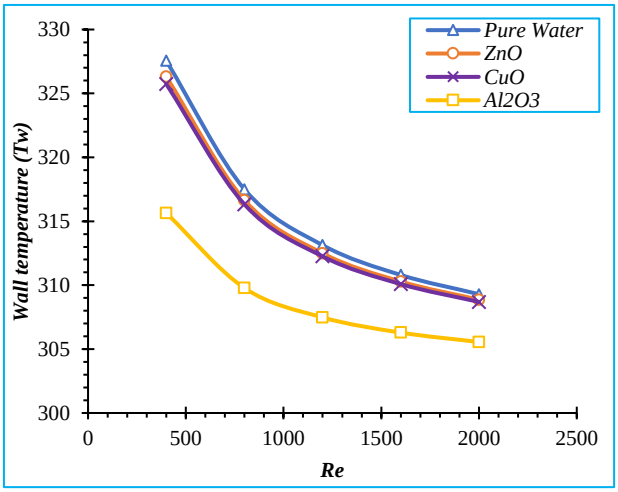

Fig. 3. MCHS T_w vs Re for $\phi = 4\%$, $d_{np} = 25\ nm$ and $h_p = 6\ \mu m$

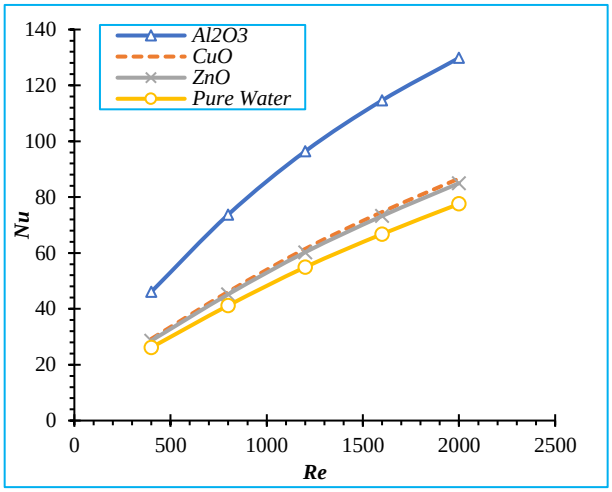

Fig. 4. Nu vs Re for $\phi = 4\%$, $d_{np} = 25\ nm$ and $h_p = 6\ \mu m$

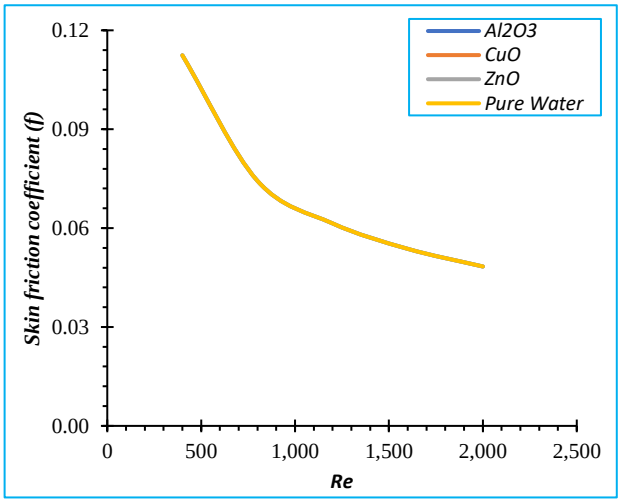

Fig. 5. f vs Re for $\phi = 4\%$, $d_{np} = 25\ nm$ and $h_p = 6\ \mu m$

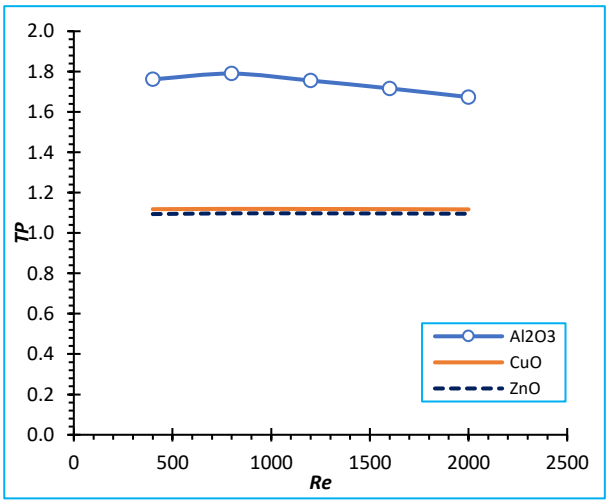

Fig. 6. TP vs Re for $\emptyset = 4\%$, $d_p = 25nm$ and $h_p = 6\mu m$

4.4 Influence of Protrusion Height

Figs. 7 through 10 illustrate the effects of protrusion height (h_p) on the wall temperature (T_w), relative Nusselt number (Nu/Nu_R), and the relative skin friction coefficient (f/f_o) using Al_2O_3 NAN with a volume fraction of 4% and a nanoparticle size of 25 nm. Fig. 7 reveals the variation of T_w with Reynolds for different protrusion depths. For all the protrusion heights and the MCHS without protrusion, the MCHS T_w decreases by increasing the Re from 400 to 2 000. In addition, T_w decreases with increasing protrusion height. The lowest MCHS T_w is reported at 6 μm, whilst an MCHS without protrusion exhibits the highest MCHS T_w. This simply implies that heat transfer is enhanced in MCHS embedded with protrusions. At $Re = 400$, MCHS T_w decreased by 4%, 3.2%, 2.4%, 1.6%, 0.8% for protrusion heights of6 μm, 5 μm, 4 μm, 3 μm, 2 μm, and 1 μm, respectively. As presented in Fig. 8, for all depths of the protrusion, the Nu/Nu_R rises with an increase in Re. A protrusion height of 6 μm depicts the highest value of Nu/Nu_R, whereas, 2 μm, has the least value of Nu/Nu_R. At $Re = 2\,000$, the protrusion heights of 6 μm, 5 μm, 4 μm, 3 μm, 2 μm, and 1 μm has about 2.65, 2.44, 2.25, 2.07 and 1.83 times the Nu of MCHS without protrusion, respectively. This means that the convective heat transfer can be improved by embedding protrusion into the MCHS. Fig. 9 relates the relative friction factor (f/f_o) to the Reynolds number for different protrusion heights. For all the protrusion heights, the f/f_o gradually increases with Re. Increased friction gives rise to an increasing relative friction factor as the height of the protrusion increases. At $400 \leq Re \leq 2\,000$, 6 μm depicts the highest value of relative friction factor, followed by 5 μm, 4 μm, 3 μm whilst 2 μm has the least value of the f/f_o. Thermal performance (TP) is deduced from the ratio of Nu/Nu_R to f/f_o. Fig. 10 illustrates the variation of thermal performance (TP) with Reynolds number (Re) for all the protrusion heights at $\phi = 4\%$, and d_p=25 nm. As revealed in Fig. 10, the (TP) increases with an increase in Re for all cases of protrusion height. For $h = 2\ \mu m$, TP is uniformly varied with Re, whereas for $3\ \mu m \leq h \leq 6\ \mu m$, a steep increase is observed at $400 \leq Re \leq 800$ as compared to gradual increase at $800 \leq Re \leq 2\,000$. More so, TP increases as protrusion height increases from 2 μm to 6 μm. A protrusion height of 6 μm yields the highest value of TP, while 2 μm gives the lowest value of TP. At $Re = 2\,000$, the TP for 2, 3, 4, 5, and 6 μm is 1.59, 1.68, 1.77, 1.86, and 1.96 times that of pure water, respectively.

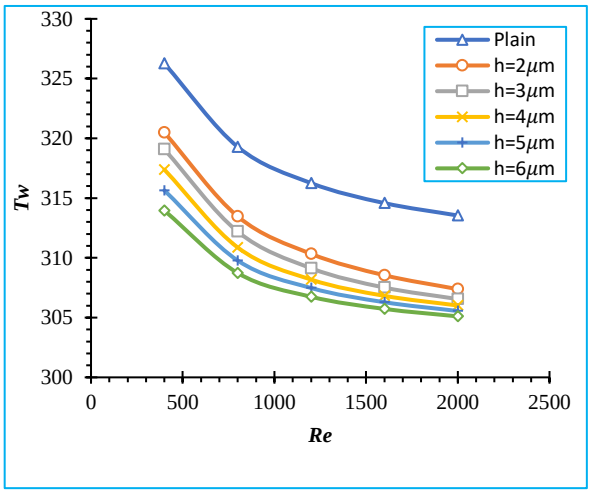

Fig. 7. MCHS wall temperature T_w with Re for $\phi = 4\%$, $d_{np} = 25\ nm$ and $z = 100\ \mu m$

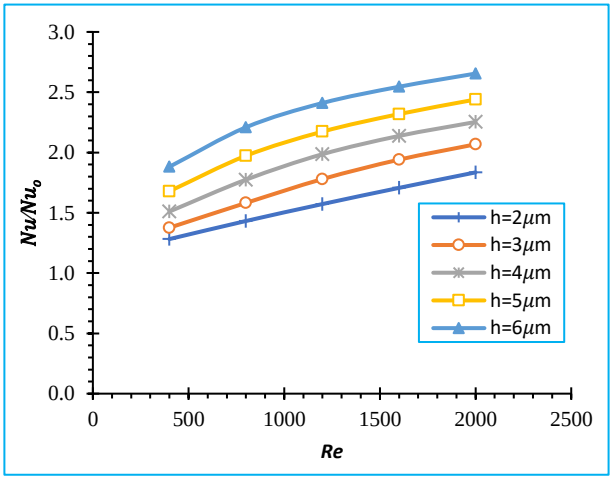

Fig. 8. Nu vs Re at $d_{np} = 25\ nm$ for $\phi = 4\%$

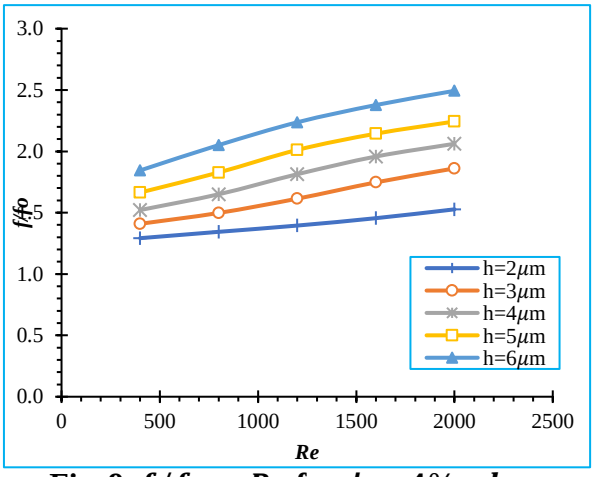

Fig. 9. f/f_o vs Re for $\phi = 4\%$, $d_{np} = 25\ nm$

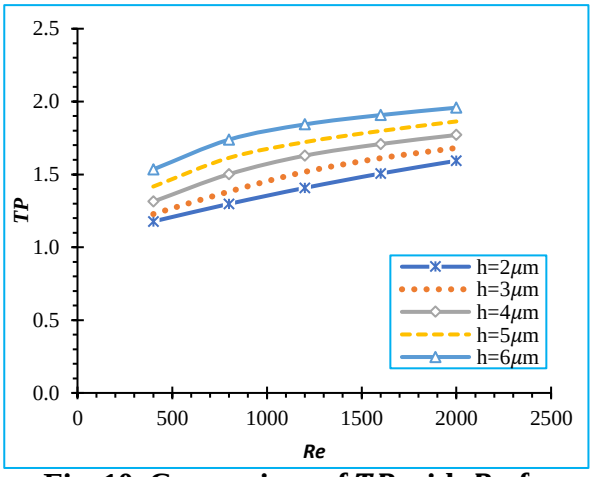

Fig. 10. Comparison of TP with Re for $Al_2O_3/water\ NF, \phi = 4\%$ and $d_{np} = 25\ nm$

4.5 Influence of Volume fraction

Figs. 11 through 14 illustrate the effect of volume fraction ($\emptyset$) from 0% to 4% of Al_2O_3 nanoparticles with a mean diameter of 25 nm on MCHS wall temperature (T_w), Nusselt number (Nu), skin friction coefficient (f), and thermal performance (TP). Fig. 11 reveals that increasing the volume fraction of the nanoparticles causes the T_w of the MCHS to reduce. At $Re = 400$, a 4% volume fraction of Al_2O_3-water NAN reduces the MCHS wall temperature by 3.6%, whereas 3%, 2%, and 1% volume fractions reduce the T_w by 2.82%, 2.13%, and 1.23%, respectively. Similarly, Fig. 12 indicates that a 4% volume fraction of Al_2O_3 nanoparticles give the maximum value of Nu because of the increased viscosity and thermal conductivity of the fluid, which subsequently enhances the heat transfer rate, whereas pure water gives the least value of Nu. At $Re = 2\,000$, 4%, 3%, 2%, and 1% volume fractions of NAN produce about 1.65, 1.51, 1.36, and 1.19 times the Nu of pure water. Fig. 13 shows that there is no change in the f observed for all volume fractions of the NAN. Fig. 14 illustrates how thermal performance is influenced by the volume fraction of the NAN. TP increases as the volume fraction increases from 1% to 4%. However, highest value of TP is obtained by using a 4% volume fraction of the nanoparticles.

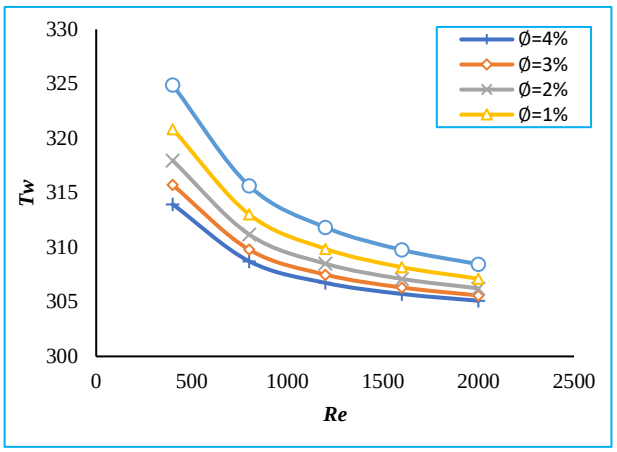

Fig. 11. MCHS wall temperature (T_w) vs Re for various $\emptyset$ of $Al_2O_3 - water$ NAN, $d_{np} = 25\ nm$

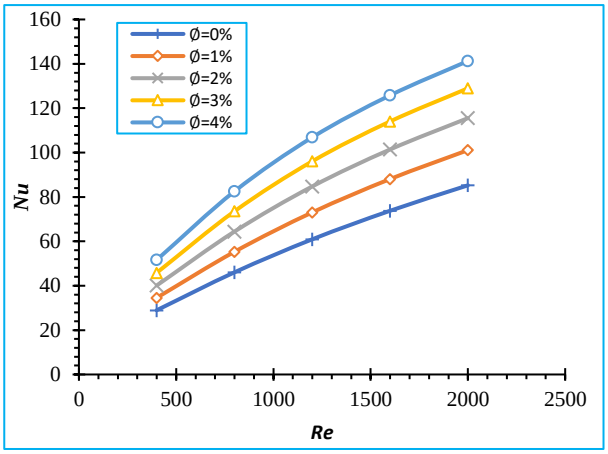

Fig. 12. Nu vs Re for $Al_2O_3 - water$ NAN at $d_{np} = 25\ nm$ for all $\emptyset$

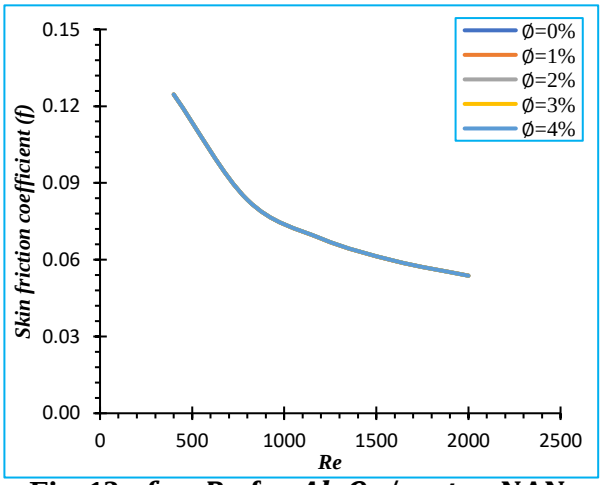

Fig. 13. f vs Re for $Al_2O_3/water$ NAN, $d_{np} = 25\ nm$

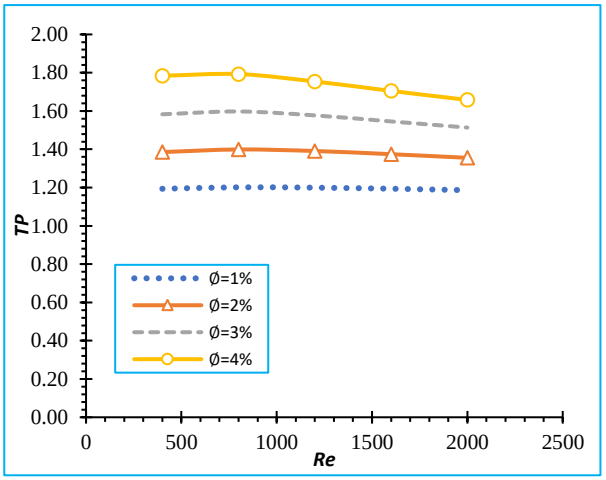

Fig. 14. TP vs Re for $Al_2O_3/$ $water$ NAN, $h = 6\ \mu m$, and $d_{np} = 25\ nm$

4.6 Temperature Contour

Fig. 15 shows the temperature contour along the x-y plane at the exit of the MCHS to visualize the effect of different nanofluid types at $Re = 1\,000$, $\phi = 4\%$ and $d_p = 25\ nm$. The temperature of the fluid at the center of the MCHS is 300 K and increases as it moves toward the wall. This is because the fluid is heated onward from the MCHS wall where constant heat flux is applied. Because of the increase in surface area, the temperature at the wall side of the protrusion is lower than the temperature of the surrounding wall of the MCHS for all cases of nanofluid. Individually, the lowest MCHS wall temperature is reported in the case of Al_2O_3 NAN as compared to other NANs while pure water has the highest MCHS wall temperature. Al_2O_3 NAN provides a maximum wall temperature of 306.1 K, CuO, ZnO NAN and pure water give maximum wall temperature of 310.2 K, 310.3 K, and 310.9 K respectively. Fig.16 presents the distribution of the temperature along the x-z plane of the MCHS of various protrusion heights. As shown in Fig. 16, the temperature at the center of the MCHS is approximately 300 K from the inlet to the outlet but varies along the wall. The maximum temperature is observed at the exit along the wall because the temperature of the fluid increases as it approaches the exit of the MCHS, and the temperature increases along the wall from the inlet to the outlet of the MCHS. Heat transfer is efficiently enhanced in protrusion height of 6 μm where its temperature at the exit along the wall is very low compared to other

protrusion heights and MCHS without protrusion due to large surface area of the protrusion. The protrusion height of 6 μm, 4 μm, 2 μm, and MCHS without protrusion provides the maximum temperature of 306.2 K, 307.3 K, 308.8 K, and 315.5 K, respectively.

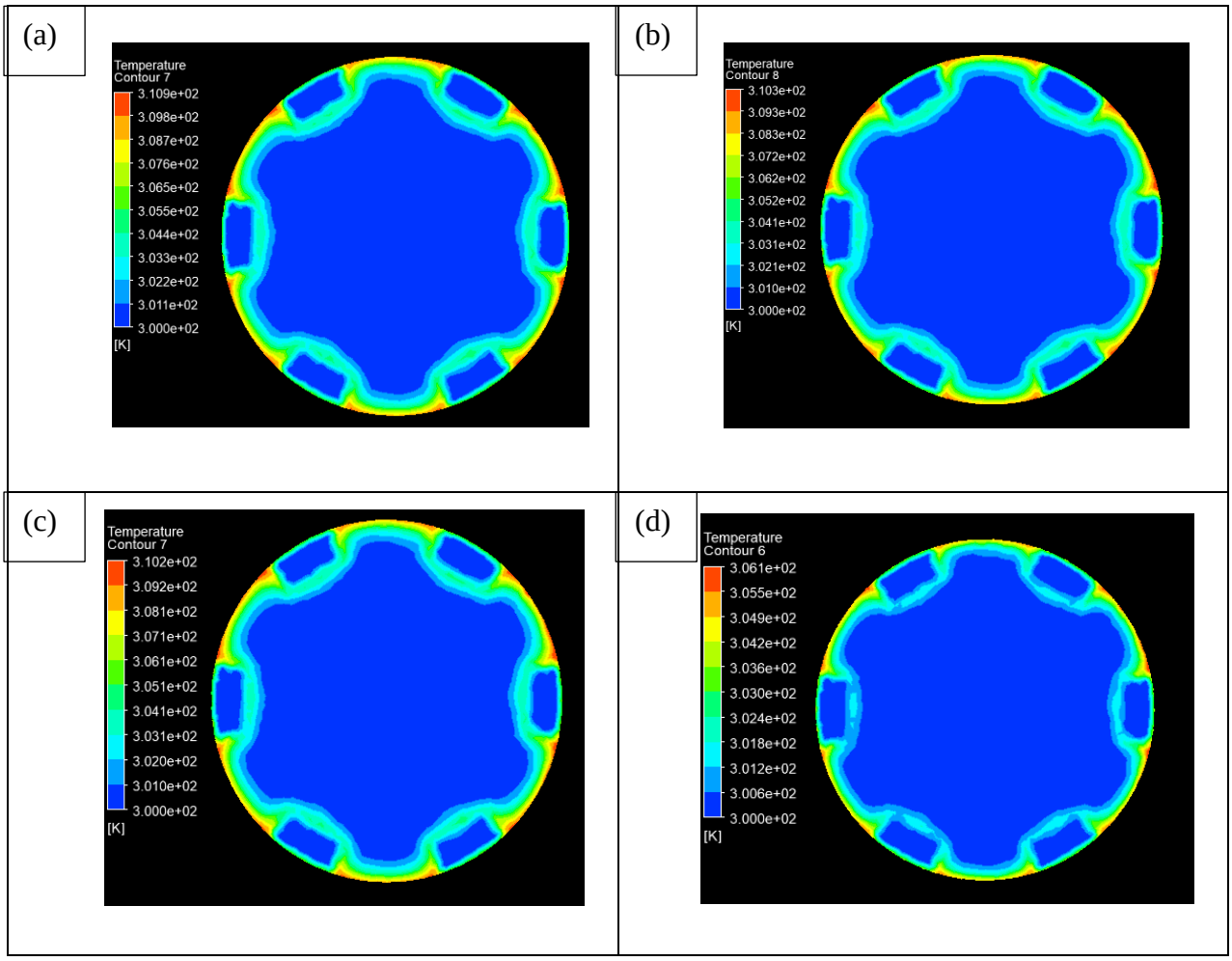

Fig. 15. Temperature contour along x-y plane at $z = 100$ µm for $h = 5$ µm, $Re = 1\,000$, $\phi = 4\%$, $d_{np} = 25$ nm for (a) Pure water (b) ZnO/water (c) CuO/water (d) Al_2O_3/water

4.6 Velocity Contour

Fig. 16 shows that the velocity of the fluid increases as it flows towards the outlet of the channel and gradually decreases towards the wall until it finally reaches zero. The highest velocity is reported for a case of protrusion height of 6 μm whereas a MCHS without protrusion depicts the lowest velocity.

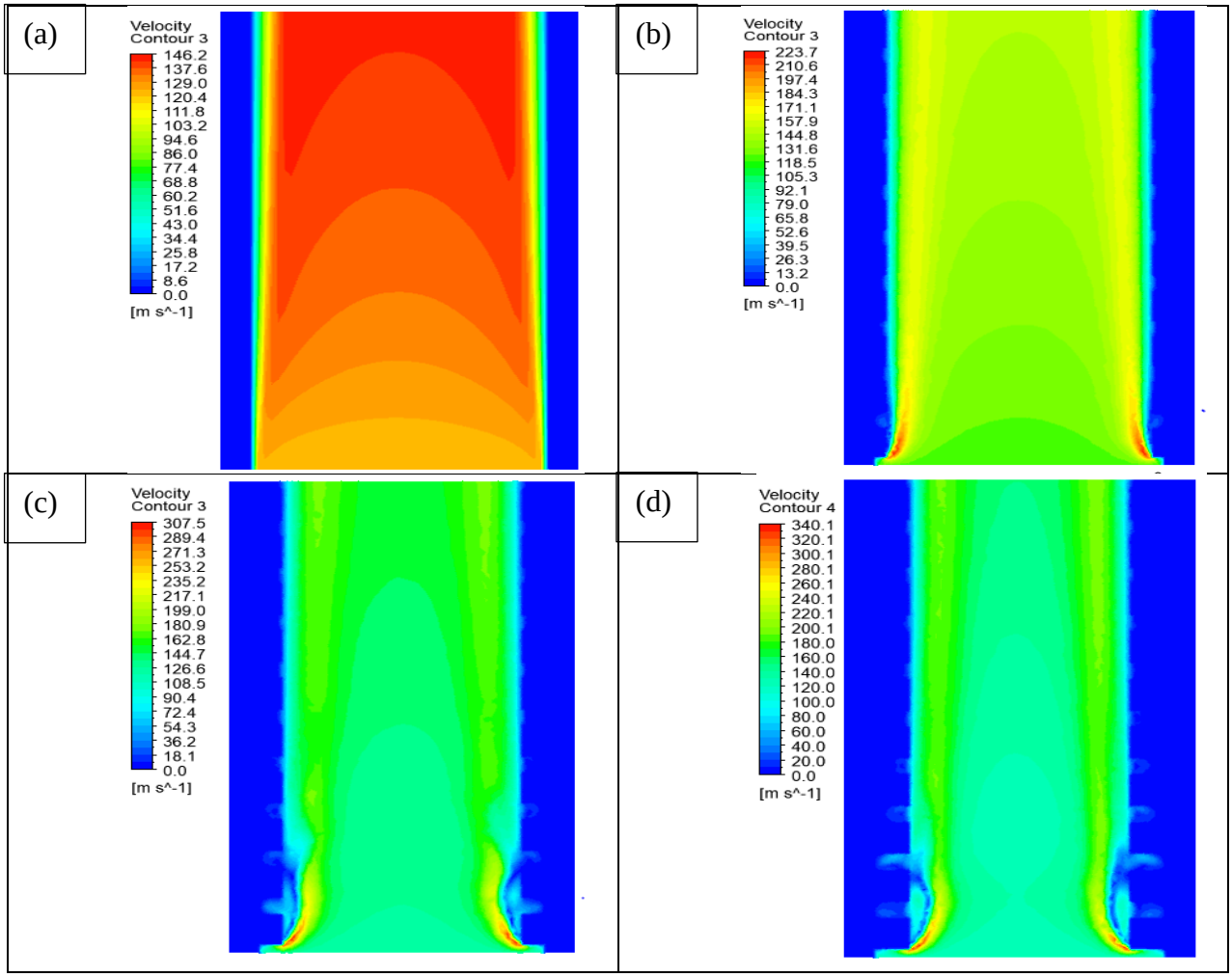

Fig. 16. Velocity contour along x-z plane for Al_2O_3 at Re = 1000, $\phi = 4\%$, and $d_p = 25nm$ for (a) MCHS without protrusion (b) $h = 2\ \mu m$ (c) $h = 4\ \mu m$ (d) $h = 6\ \mu m$

5. Conclusion

In a tubular MCHS with protrusions, the thermal performance analysis of nanofluids as cooling fluid was numerically investigated under the steady-state condition at various protrusion heights, volume fractions, and nanofluid types. The main findings are summarized below as follows:

- The addition of nanoparticles to pure water lowers the MCHS wall temperature and enhances the heat transfer rate as compared to pure water. Among the nanofluids used in this study, Al_2O_3 nanofluid provides a 40% improvement in heat transfer enhancement and a 4% reduction in the maximum temperature of the surrounding wall of MCHS.
- The presence of nanoparticles in the pure water provides no significant change in skin friction coefficient for all constant volume fractions.
- Al_2O_3 nanofluid yields better thermal performance than both CuO and ZnO nanofluid.
- Increasing the protrusion height from 2 µm to 6 µm causes the heat transfer rate and thermal performance to increase. However, the surrounding wall temperature of the MCHS decreases due to the dominating effect of the protrusion surface area; compared to the smooth tube without protrusion, at Reynolds number 2 000, the wall temperature is reduced by 4% and thermal performance is improved by 1.96 using a protrusion height of 6 µm
- As protrusion height increases from 2 µm to 6 µm, relative Nusselt number and relative friction factor increases

- As nanoparticle concentration is increasing from 0% to 4%, MCHS wall temperature reduces, and heat transfer rate increases for all types of nanofluids
- Thermal performance improves as the volume fraction of nanofluid increases from 1% to 4%.
- Skin friction coefficient does not vary in any response to the concentration of the nanofluid.

Acknowledgements

The authors appreciate the University of Lagos for their support.

References

Adham, A. M., & Mohammed, H. A. (2021). Numerical assessment of the overall heat transfer and pressure drop performances of an aqueous ammonia base-nanofluids in rectangular microchannel heat sinks. *Journal of Mechanical Engineering Research and Developments*, *44*(4), 373–380.

Ahmed, M. A., Shuaib, N. H., Yusoff, M. Z., & Al-Falahi, A. H. (2011). Numerical investigations of flow and heat transfer enhancement in a corrugated channel using nanofluid. *International Communications in Heat and Mass Transfer*, *38*(10). https://doi.org/10.1016/j.icheatmasstransfer.2011.08.013

Ali, A. M., Angelino, M., & Rona, A. (2021). Numerical analysis on the thermal performance of microchannel heat sinks with Al2O3 nanofluid and various fins. *Applied Thermal Engineering*, *198*, 117458. https://doi.org/10.1016/j.applthermaleng.2021.117458

Aurangzeb, M., Noor, F., Qamar, A., Shah, A. N., Kumam, P., Shah, Z., & Shutaywi, M. (2022). Investigation of enhancement in the thermal response of phase change materials through nano powders. *Case Studies in Thermal Engineering*, *29*. https://doi.org/10.1016/j.csite.2021.101654

Chaurasia, S. R., & Sarviya, R. M. (2021). Experimental and numerical thermal performance evaluation of helical screw inserts in a tube with double strips at laminar flow. *Computational Thermal Sciences*, *13*(1). https://doi.org/10.1615/computthermalscien.2020033915

Chon, C. H., Kihm, K. D., Lee, S. P., & Choi, S. U. S. (2005). Empirical correlation finding the role of temperature and particle size for nanofluid (Al2O3) thermal conductivity enhancement. *Applied Physics Letters*, *87*(15), 153107. https://doi.org/10.1063/1.2093936

Cong, R., Ozaki, Y., Machado, B. S., & Das, P. K. (2018). Constructal design of a rectangular fin in a mixed convective confined environment. *Inventions*, *3*(2). https://doi.org/10.3390/inventions3020027

El Bécaye Maïga, S., Palm, S. J., Nguyen, C. T., Roy, G., & Galanis, N. (2005). Heat transfer enhancement by using nanofluids in forced convection flows. *International Journal of Heat and Fluid Flow*, *26*(4 SPEC. ISS.). https://doi.org/10.1016/j.ijheatfluidflow.2005.02.004

Gong, L., Lu, H., Li, H., & Xu, M. (2016). PARAMETRIC NUMERICAL STUDY OF THE FLOW AND HEAT TRANSFER IN A DIMPLED WAVY MICROCHANNEL. *Heat Transfer Research*, *47*(2), 105–118. https://doi.org/10.1615/heattransres.2015010726

Heris, S. Z., Etemad, S. G., & Esfahany, M. N. (2006). Experimental investigation of oxide nanofluids laminar flow convective heat transfer. *International Communications in Heat and Mass Transfer*, *33*(4). https://doi.org/10.1016/j.icheatmasstransfer.2006.01.005

Khetib, Y., Abo-Dief, H. M., Alanazi, A. K., Cheraghian, G., Sajadi, S. M., & Sharifpur, M. (2021). Simulation of Nanofluid Flow in a Micro-Heat Sink With Corrugated Walls Considering the Effect of Nanoparticle Diameter on Heat Sink Efficiency. *Frontiers in Energy Research*, *9*(Article 769374). https://doi.org/10.3389/fenrg.2021.769374

Khetib, Y., Abo-Dief, H. M., Alanazi, A. K., Sajadi, S. M., Sharifpur, M., & Meyer, J. P. (2021). Computational fluid dynamics study of efficiency of a wavy microchannel heat sink containing various nanoparticles. *Micromachines*, *12*(10). https://doi.org/10.3390/mi12101192

Manca, O., Nardini, S., Ricci, D., & Tamburrino, S. (2012). Numerical investigation on mixed

convection in triangular cross-section ducts with nanofluids. *Advances in Mechanical Engineering*, *2012*. https://doi.org/10.1155/2012/139370

Marques, C., & Kelly, K. W. (2004). Fabrication and Performance of a Pin Fin Micro Heat Exchanger. *Journal of Heat Transfer*, *126*(3), 434–444. https://doi.org/10.1115/1.1731341

Masoumi, N., Sohrabi, N., & Behzadmehr, A. (2009). A new model for calculating the effective viscosity of nanofluids. *Journal of Physics D: Applied Physics*, *42*(5). https://doi.org/10.1088/0022-3727/42/5/055501

Mohamad Hafzan Mohamad Jowsey, Natrah Kamaruzaman, & Mohsin Mohd Sies. (2021). Heat and Flow Profile of Nanofluid Flow Inside Multilayer Microchannel Heat Sink | Journal of Advanced Research in Micro and Nano Engineering. *Journal of Advanced Research in Micro and Nano Engineering*, *4*(1), 1–9.

Munimathan, A., Sathish, T., Mohanavel, V., Karthick, A., Madavan, R., Subbiah, R., … Rajkumar, S. (2021). Investigation on Heat Transfer Enhancement in Microchannel Using Al2O3/Water Nanofluids. *International Journal of Photoenergy*, *2021*. https://doi.org/10.1155/2021/6680627

Pordanjani, A. H., Aghakhani, S., Afrand, M., Sharifpur, M., Meyer, J. P., Xu, H., … Cheraghian, G. (2021). Nanofluids: Physical phenomena, applications in thermal systems and the environment effects- a critical review. *Journal of Cleaner Production*, *320*. https://doi.org/10.1016/j.jclepro.2021.128573

Rhaghuveer, S. R., & Harish, S. (2021). No TitleEffect of different nanofluids flow in microchannel heat sink. *International Journal for Research Trends and Innovation*, *6*(3), 2456–3315.

Uday Kumar, A., Javed, A., Dubey -, S. K., Botez, D., Chang, C.-C., Bhattacharya, R., & Samanta, P. (2021). Simulation-based Study of Graphene-water Nanofluid flow through Microchannel Heatsink. *IOP Conference Series: Materials Science and Engineering*, *1206*(1), 012008. https://doi.org/10.1088/1757-899x/1206/1/012008

Wang, Y., Houshmand, F., Elcock, D., & Peles, Y. (2013). Convective heat transfer and mixing enhancement in a microchannel with a pillar. *International Journal of Heat and Mass Transfer*, *62*(1), 553–561. https://doi.org/10.1016/j.ijheatmasstransfer.2013.03.034

Yan, S. R., Aghakhani, S., & Karimipour, A. (2020). Influence of a membrane on nanofluid heat transfer and irreversibilities inside a cavity with two constant-temperature semicircular sources on the lower wall: applicable to solar collectors. *Physica Scripta*, *95*(8), 085702. https://doi.org/10.1088/1402-4896/ab93e4